Investigation of the Structural Performance of Masonry Wharf Cellars in Utrecht Using the Distinct Element Method

Yopi Oktiovan(✉), Anjali Mehrotra, Francesco Messali, and Jan Rots

Department of Materials, Mechanics, Management & Design, Faculty of Civil Engineering and Geosciences, Delft University of Technology, 2628 CN Delft, Netherlands
y.p.oktiovan@tudelft.nl

Abstract. One of the characteristic features of the city of Utrecht is its extensive system of canals and wharf cellars, whose constructions date back as early as the 1200s, and which are now considered as one of the historical properties of the city. A typical wharf cellar in Utrecht comprises a masonry barrel vault with multi-layered rings for the cellar interior, masonry piers which are interconnected to the other wharf cellars, and spandrel walls for the façades. Due to increased traffic volume and urbanization which caused the increase of dead load and traffic load, it is important to assess the structural safety and state of maintenance of these historical structures. In this paper, a novel safety assessment framework for these structures is presented and applied to the analysis of a typical masonry wharf cellar in central Utrecht. The geometry of the cellar is first parametrically generated, which is then used to create a block-based numerical model for analysis using the Distinct Element Method (DEM), where bricks units are modelled as discrete blocks separated by zero thickness interfaces. Traffic loads in accordance with the Dutch Standard traffic model for regular vehicles and emergency service vehicles are calculated and the dispersion through the filling soil is modelled. The ultimate load due to these load configurations is then assessed. The analysis results can be used to identify the critical load cases and the failure mechanisms of the wharf cellar, while also providing general insights into the safety and stability of the cellars, thus aiding engineers in their efforts to extend the lifespan of these historical structures.

Keywords: Utrecht Wharf Cellar · Distinct Element Method · Traffic Load · Barrel Vault · Boussinesq theory

1 Introductions

Masonry arches and vaults have been the basis of the structural elements for many historical constructions since the first ever known masonry arched structures in ancient Egypt and Mesopotamia. The number of masonry arched structure in Europe is estimated to be more than 200,000 within the railway network and is predicted to reach 300,000 if the masonry bridges within the public road system are taken into account [1]. In the

© The Author(s), under exclusive license to Springer Nature Switzerland AG 2024
Y. Endo and T. Hanazato (Eds.): SAHC 2023, RILEM Bookseries 46, pp. 287–300, 2024.
https://doi.org/10.1007/978-3-031-39450-8_24

Netherlands, a large part of the public road network is still connected to masonry arch bridges and vaults, whose construction dates back to the Middle Ages. These structures still serve as functional infrastructures subjected to relatively large traffic loads every day. The city of Utrecht in the Netherlands is well known for its wharf and street cellars which were built starting from the twelfth century and are now integrated to the public roads. The cellars were initially built to store goods that were transported from the canals. Nowadays, they are used as terraces, office spaces, and other economic functions. The cellars are also considered as one of the historical properties of the city under the National Monument *Stadsbinnengrachten en Werven.*

The construction of the wharf cellar and its typical components are shown in Fig. 1a and Fig. 1b, respectively. The numbers in Fig. 1b are described as follows; 1: cellar's vault, 2: basement foundation and retaining walls, 3: cracks and leakage, 4: street traffic, 5: wall anchors, 6: basement access, 7: water drain, 8: cable pipes, 9: waterproof layer, 10: new waterproof layer, and 11: wall façades. A typical cellar system comprises a longitudinal bond barrel vault, cross bond masonry piers interconnected to adjacent wharf cellars, and a spandrel wall for the façade. Depending on the span of the cellar system, multi-ring arrangements are used on the cellar's vault. Due to urbanization and increased traffic volume, the loads sustained by these structures have changed from pedestrian, horses, and carriages to heavier motorized vehicles.

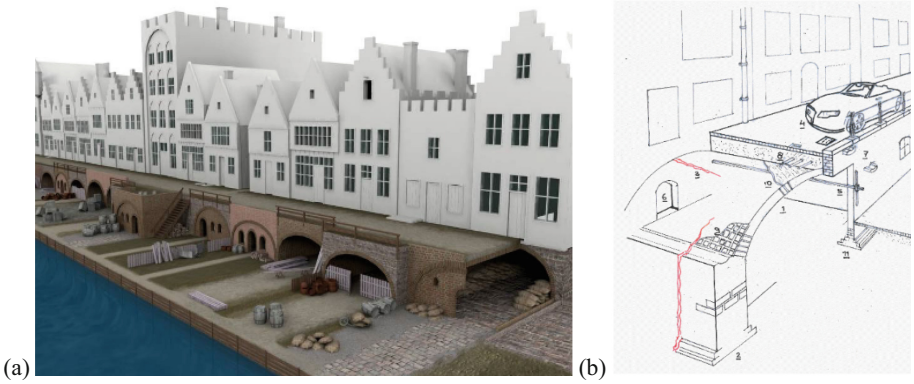

Fig. 1. Sketches of (a) construction of wharf with wharf cellars and (b) wharf cellars typical components [2]

Furthermore, the recent collapse of the historical Grimburgwal quay wall in Amsterdam [3] brought to light the importance of assessing the structural safety and state of maintenance of historical structures in Dutch cities. A collaborative work between Witteveen + Bos, Antea Group, and Royal Haskoning DHV for the municipality of Utrecht was started in 2021 to assess the load bearing capacity, investigate the causes of damage in the defective cellars, and check the maximum permissible load for the traffic to safely cross the wharf cellars [2]. The study utilized two-dimensional numerical modelling of the wharf cellar system and the surrounding soil to assess the safety of the cellar in

accordance with the NEN 8701 Dutch guideline for assessment of existing structures. [4].

The assessment method of the load bearing capacity and serviceability limit of arched structures have been extensively studied, from the empirical MEXE method to non-linear numerical methods such as finite or discrete element methods. Sarhosis, *et. al.* [5] summarized the experimental investigations and assessment method for masonry arch bridges but can be easily extended to vault structures as well. Typically for fast and reliable results, empirical methods or limit state based approaches are enough to obtain the collapse load and reactions of the abutments/piers. However, the load bearing capacity seldom overestimated due to the imposed assumptions and information about the displacements and stress distributions are not provided. Recently with the increase of computational power, researchers have leaned into utilizing a micro modelling strategy called distinct element method (DEM) where masonry units are represented as assemblages of block units and mortar joints represented as zero thickness interfaces. This method is widely used for the assessment of masonry arched structures [6, 7, 8].

In this context, this paper introduces a safety assessment framework based on the micro modelling approach and demonstrates it via application to the compliancy assessment of an Utrecht wharf cellar as a case study. The numerical framework utilizes a rigid block formulation where nonlinearities and block deformations are lumped at the interfaces between blocks. The compliancy of the wharf cellar model is checked against the load model in accordance to the Dutch Guideline for traffic loads on bridges and other civil engineering works [9]. If the structure is compliant, the applied load is incrementally increased until failure is reached and the failure mechanism and ultimate load bearing capacity of the cellar is observed. The failure load and mechanism obtained from the numerical model will enable engineers to check the safety and stability of the cellars in their efforts to extend the lifespan of the historical structure.

2 Case Study of the Wharf Cellar in *Kromme Nieuwegracht*

The wharf cellar system shown in the right-hand side of Fig. 2a is located in the *Kromme Nieuwegracht* canal in the center of Utrecht. The cellar was built possibly in the 12th century, and then rebuilt between 1500–1700 with a higher crown height. The wharves were used as ground-level transport of goods and the cellars were used for storage. The cellar system used for the demonstration of the proposed framework comprises three inter-connected wharf cellars which consist of masonry barrel vaults and load bearing walls with varied springing level. The cross-section drawing of the cellar system is presented in Fig. 2b. The units shown are in mm.

The geometrical information is summarized in Table 1 based on the investigation report conducted by Royal Haskoning DHV [10], hereby termed as the investigation report,. The heights were measured based on the N.A.P (*Normaal Amsterdams Pell* / Normal Amsterdam Level), a reference plane for height in the Netherlands. The interior height is measured between NAP + 2.946 mm and NAP + 2.969 mm. The foundations of the cellar system (below the NAP 0.0 m) are shallow foundations sitting on a loosely packed sand.

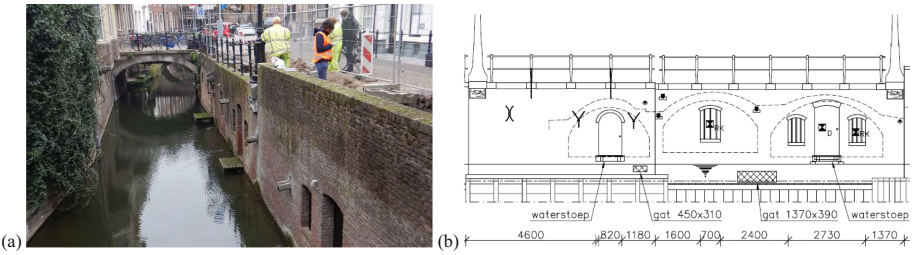

Fig. 2. (a) existing situation and (b) cross-section of a reference wharf cellar in Utrecht (all units in mm) [10]

Table 1. Geometrical data of *Kromme Nieuwegracht* Wharf Cellar

Kromme Nieuwegracht		Piers		Arch	
Total Length	12.88 m	Width	1.4 m	Span	4.8 m
Height over the N.A.P	3.34 m	Length	4.2 m	Rise at midspan (NAP +)	2.73 m
Number of Arches	3	Height (NAP +)	2.6 m	Vault depth	0.26 m

The material properties, presented in Table 2, are based on the characteristic values specified in the NPR 9998 + C1:2020 [11], the Dutch practical guideline for safety assessment of buildings. The density of the masonry is taken as 23 kN/m^3 while the backfill and pavement density are taken at 18 kN/m^3 and 23 kN/m^3, respectively. The dilatancy angle is assumed equal to 0. The cross-section of the barrel vault was identified by drilling two boreholes at the highest point of the vault. The drill core result showed that the barrel vault consisted of one brick unit stacked upright with dimensions of 220 × 110 × 55 mm (Length x Width x Height) and another unit stacked horizontally perpendicular to the previous layer, with mortar thickness of approximately 10 mm.

Table 2. Masonry material properties as per Table F.2. of NPR 9998 (2020) [11]

Properties	Table F.2 NPR 9998 (2020)	Masonry Clay Brickwork (pre 1945)	Units
Elastic modulus	E_m	6000	N/mm^2
Shear modulus	G_m	2500	N/mm^2
Uniaxial tensile strength	$f_{ma;b;per}$	0.1	N/mm^2
Initial bed joint shear strength	$f_{ma;v;0}$	0.3	N/mm^2
Bed joint shear friction coefficient	$\mu_{ma;m}$	0.75	[-]

The illustration of the vault's cross-section and the investigation footage are presented in Fig. 3a and Fig. 3b, respectively. Finishing layers were found at the top and bottom side of the vaults, while a bituminous layer for waterproofing was observed at the top-side. The total vault thickness excluding the finishing layers was 260–270 mm. A cross bond pattern was found at the location of the piers while a longitudinal bond pattern was observed at the vaults. The transition occurred at the springing level, approximately NAP + 1.9 m. According to the investigation report, the assessment results for special traffic load showed that there was a risk of crack formation perpendicular to the direction of travel where the tensile strength at the bottom and top of the arch was exceeded even though the collapse load was considerably higher.

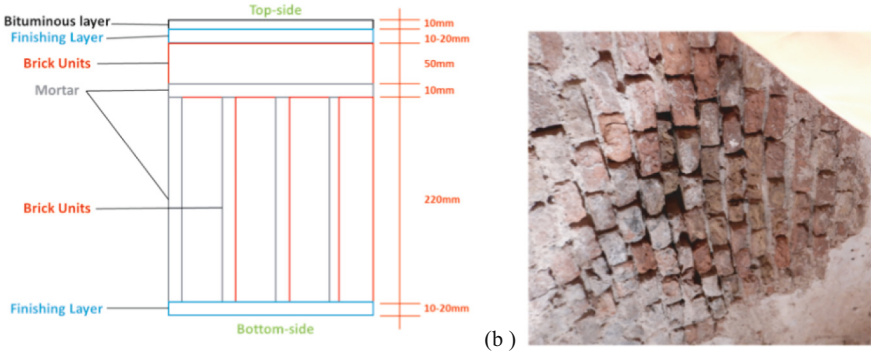

Fig. 3. (a) Illustration of the cellar vault's cross-section and (b) Investigation footage at the bottom of barrel vault

3 Distinct Element Modelling of Utrecht Wharf Cellar

The presented wharf cellar system is then modelled based on the three-dimensional distinct element method (DEM) [12] using the commercially available software *3DEC* 7.0 [13]. This numerical method has been extensively used in the numerical analysis of arched structures and is particularly useful to this research to observe the failure mechanism and damage propagation of the cellar system at a detailed level. In DEM, the masonry blocks are modelled as assemblages of rigid or deformable blocks connected via point contacts comprising interface springs. Interactions between distinct blocks are defined using the *soft-contact* approach, which allows interpenetration between blocks, the extent of which is controlled by the stiffness of the interface springs. The equation of motion in DEM is solved using an explicit time-marching scheme where central difference algorithm is used. For static problems, the convergence or failure mechanism is reached by introducing dynamic relaxation, a form of artificial damping, to the equation of motion. [14].

The flowchart outlining the block generation and numerical analysis for the safety assessment tool is presented in Fig. 4. The process starts with the parametric generation of the cellar system geometry in *Rhino* + *Grasshopper* based on the inputs from Table 1

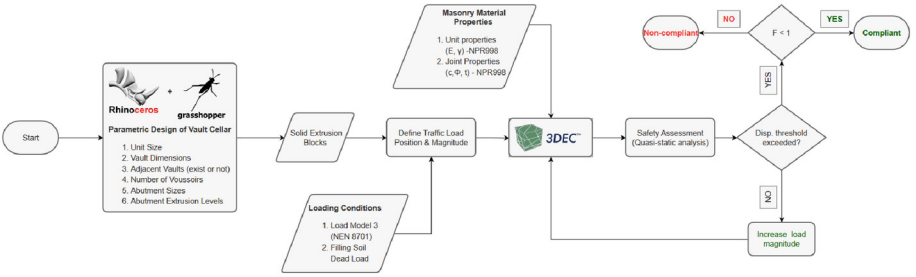

Fig. 4. Flowchart of the block generation and analysis for the safety assessment of Utrecht Wharf Cellar model

and on-site inspection. The parametric geometry generation tool contains a series of *Grasshopper* components with ad-hoc C# scripts that allows fast and robust generation of vault masonry blocks including the longitudinal bond pattern at the barrel vault. Note that the masonry units are modelled with extended dimensions up to half of the mortar joint thickness on all sides of the units. The crown height of the arch elements is uniform for the sake of modelling simplicity. In order to save computational time and reduce the number of blocks modelled, only half of the left and right cellars are defined. The generated geometry is presented in Fig. 5a. In order to retain the joint plane (face-to-face contact) between the vertical units and horizontally stacked units (which in reality would be realized via the layer of mortar), the horizontally stacked units are further discretized into three distinct elements corresponding to the contacting vertical units below them as shown in Fig. 5b.

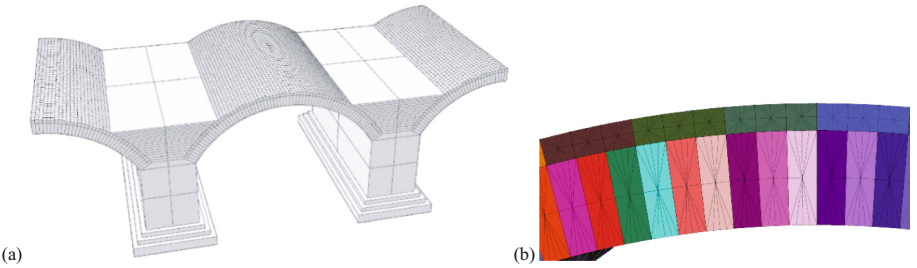

Fig. 5. (a) Isometric view of the Rhino 3D model of Utrecht Wharf Cellar and (b) stacking pattern at the arch section

The blocks are then imported into *3DEC* and contacts between each of the cellar elements are defined. The blocks are modelled as rigid, while all deformation is lumped into the interface springs. Block density is the only unit input parameter needed under rigid blocks formulation. A Coulomb friction joint constitutive model is applied to the contacting points of the blocks where material properties in Table 2 are used as the joint properties, with zero dilation angle. The joint normal and shear stiffnesses at the contacts between blocks are defined as a function of Young moduli of brick units and mortar over the contact area, as presented in Eq. (1) and Eq. (2) for normal and shear joint stiffness,

respectively [15]:

$$k_n = \frac{E_b \cdot E_m}{(E_b - E_m)xh_j} \tag{1}$$

$$k_s = \frac{k_n}{2(1+v)} \tag{2}$$

where E_b and E_m are the brick and mortar Young's moduli, h_j is the joint height and v is the Poisson's Ratio.

In terms of boundary conditions, the bottom of both piers are fixed, and in order to simulate symmetric conditions at both ends of the arch vaults, non-physical rigid blocks are defined where blocks are fixed and frictionless contact joints are applied between the blocks and the vault elements. Once the masonry material properties are defined, the *3DEC* model is brought to equilibrium under gravity load. Then, the fill material above the cellar system is added as dead load and also brought to equilibrium.

The traffic load in accordance with the BM3 of the NEN-EN 1991–2/NB guideline [9] is applied incrementally until the full application of the load. If after full application of the load, the maximum displacement of the structure is still within the specified threshold by the Dutch guideline, which in this case equals to 0.032m, the structure is considered compliant under the applied load. To obtain the failure load, the traffic load is then incrementally increased beyond the full application of the load until collapse occurs to determine the failure load of the cellar system. The failure load is determined when the F (capacity /demand) ratio in Fig. 4 is less than 1, or when the observed displacement keeps increasing to infinity.

The backfill load on the arch can be represented as irregularly shaped particles, e.g. Voronoi shape, or be represented as a distributed load over the area. However, with the rigid block formulation in *3DEC*, only the latter option is allowed. Since the backfill soil is not explicitly defined in this model, the traffic loads are applied similarly as distributed loads. The load dispersion model follows the Boussinesq distribution [16] along the arch ring while the load is uniformly distributed if it extends beyond the arch ring. By assuming a semi-infinite elastic soil below the level surface, the load dispersion is defined by Eq. (3). The angle definition is presented in Fig. 6. Note that the angles in Eq. (3) are in radians.

$$\sigma_z = \frac{q}{\pi}[\alpha + \sin\alpha\cos(\alpha + 2\beta)] \tag{3}$$

The assessment approach by Royal Haskoning DHV [10] prescribed eight positions along the travel direction of the wharf cellar. In this paper, the heaviest axle load will be applied at the center of the middle wharf cellar (position #5 in the investigation report). The other positions will be validated as part of the future work of this paper. The BM3 load model in accordance with NEN-EN 1991–2/NB is based on a traffic load in case of emergency deployment of fire services. The ladder fire truck is chosen for the safety assessment since the truck has the heaviest axle load weight. The ladder truck has two axles of 8 tons and 11.5 tons with an axle-to-axle distance of 4.2 m. The rear axle is applied at the center of the middle cellar while the front axle is applied closer to the left

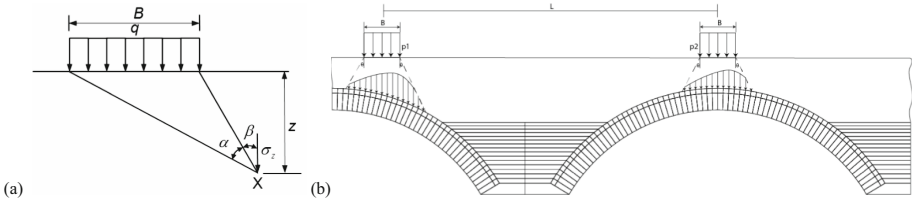

Fig. 6. Illustration of (a) Boussinesq distribution and (b) Traffic load dispersion

cellar since the cellar system was located in a one-way traffic lane with the direction travel going from the right cellar to the left.

According to NEN-EN 1991–2/NB, a magnification factor of 1.4 must be considered when the special vehicles move at a speed of more than 5 km/h. Therefore, the distributed loads for the rear and front axles are 1.4*115kN/(4.2*1.0) = 38.3 kN/m^2 and 1.4*80kN/(4.2*1.0) = 26.7 kN/m^2, respectively. Illustration of the load application for BM3 is presented in Fig. 6b. The traffic load dispersion along the arch ring is limited by an angle of dispersion at both ends of the area load. The angle of dispersion, θ, is set to 30° according to Chapter 4.9.1 of NEN-EN 1991–2/NB. The example of the load application in the middle arch is shown in Fig. 7. Once the traffic load magnitude is defined, the area of the arch model that falls within the area limited by the angle of dispersion, the violet arrows in Fig. 7, is searched. The dispersed traffic area load calculated using Eq. (3) is then distributed to the nodes (grid-points) of the blocks within the area.

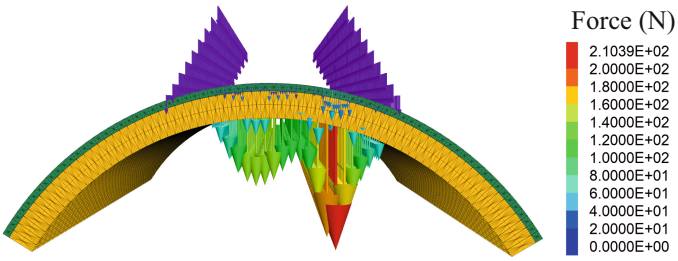

Fig. 7. Example of traffic load application in the middle arch of the wharf cellar model (BM3 load)

Based on the site inspection report [10], layers of loose sand were found below the floors of the wharf cellar system. Therefore, a lateral earth pressure also needs to be considered as an additional load acting on the cellar system. Similar to the backfill load, since the soil below the floors is not modelled, the lateral earth pressure loads on the piers are applied as displacement-dependent distributed loads, according to the unified model by Ni, *et. al.* [17]. The lateral pressure load takes the relative displacement of both sides of the pier, converts it to the coefficient of lateral earth pressure and multiplies the coefficient by the unit weight and the soil depth. The lateral load is applied uniformly at the piers.

4 Analysis Results

4.1 Safety Assessment of *Kromme Nieuwegracht* Wharf Cellar System Under BM3 Load

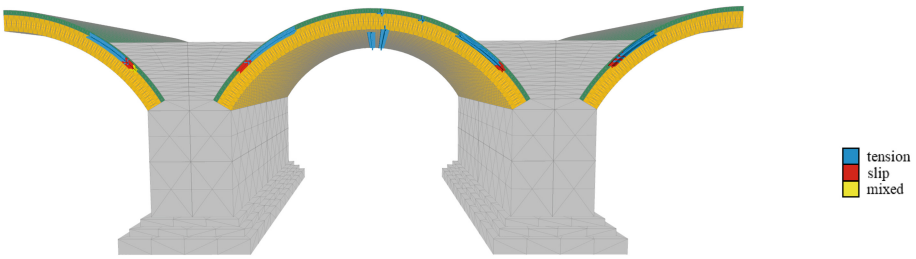

Fig. 8. Damage state of the wharf cellar model after 100% application of BM3 load

The quasi-static analysis for load model BM3 managed to reach 100% application of the load with minimal damage. The damage state of the wharf cellar model after 100% application of BM3 load is shown in Fig. 8. The damage started with tensile separation on the interfaces between the vertically (orange-coloured) and horizontally (green-coloured) stacked units, specifically at the region close to the piers before the 100% application of the load. As the analysis underwent the 100% load application, the separation of the bed joints at the centre of the middle arch occurred, which is consistent with the findings from the investigation that there was crack formation on the cellar vault perpendicular to the direction of travel. Note that the damage state in *3DEC* occurs when the corresponding strengths (tensile/shear) are exceeded.

The maximum displacements at every load increment of each arch is shown in Fig. 9a. The maximum displacement is obtained after equilibrium is reached at the end of each load increment. It can be seen that even after 100% application of BM3 load, the displacement response of the cellar system under traffic load and dead load is linear. It is also important to note that the sudden change of stiffness occurred due to the fact that the backfill load application stage was also included in Fig. 9a (until the total load reached 13.3kN). Meanwhile, the joint normal displacement vectors at the middle arch of the wharf cellar model is presented in Fig. 9b. Even though the normal displacement is relatively small, the separation between the pier and arch has occurred since the tensile damage state has been recorded.

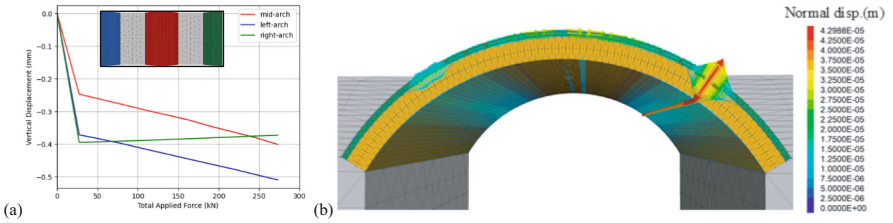

(a) (b)

Fig. 9. (a) vertical displacement vs total applied force and (b) normal displacement vector at middle arch of the wharf cellar model

The calculated displacement requirement in accordance with NEN 9997–1:2016 is found to be 0.032 m. Comparing the required displacement against the maximum observed displacement from the numerical analysis, it can be concluded that the wharf cellar structure in *Kromme Nieuwegracht* is compliant under the BM3 load model of the NEN-EN 1991–2/NB Dutch guideline when the heaviest axle load is applied at the crown height of the middle arch. Note that different positions and load scenarios are beyond the scope of the present paper, but will be considered as part of the future work of this research. Validation of the cellar model against the site inspection results or other numerical methods such as limit state analysis or finite element analysis are also envisioned.

4.2 Failure Load and Failure Mechanism of *Kromme Nieuwegracht* Wharf Cellar Model

After the compliancy of BM3 load model in accordance to NEN-EN 1991–2/NB is confirmed, the next step is to find the failure load and the governing failure mechanism. Considering the same loading position as specified in Sect. 4.1, the load is increased beyond the full application of BM3 until failure occurs. Failure occurs when the observed displacement keeps on increasing to infinity. It is observed that there is a significant capacity until failure occurs at the cellar system.

The damage state of the wharf cellar model at failure load is presented in Fig. 10. It can be seen that the initial separation between vertically and horizontally stacked units were more apparent at failure where separations extended from the springing level up to the highest point of the pier that was in contact with the arch units (Fig. 10a and Fig. 10b). Furthermore, the damage mechanism also changed between the left side and right side arch as it extended towards the crown of each arch. Sliding failure between the vertical and horizontal units was observed on the left arch, while separation failure was found on the interfaces between the arch units of the right arch. Combined sliding-separation failure was also found between the bed joints of the horizontal units on the right-side arch. A similar damage pattern was observed at the middle arch (Fig. 10c) where separation failure at the interfaces of the arch units are continuous from one side of the pier to another. Sliding-separation failure was found towards the depth of the cellar at the area where the traffic load was applied.

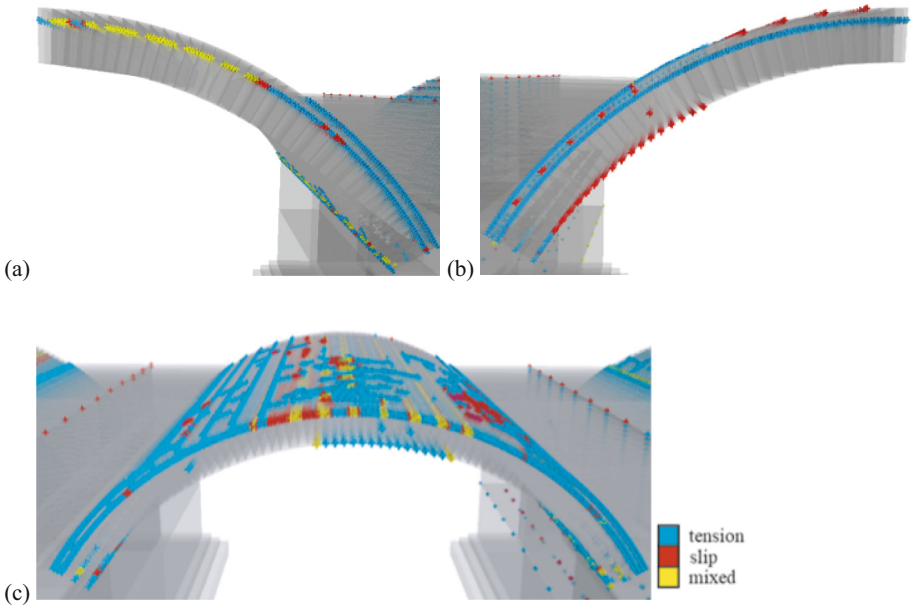

Fig. 10. Damage state of the wharf cellar under failure load condition at (a) left arch, (b) right arch, and (c) middle arch

The maximum displacement versus the total applied force until failure is presented in Fig. 11a. It is evident that until the onset of the failure load, the displacement response on all arches is relatively stable and as failure occurs the displacement increases significantly. On the middle arch where the heaviest axle load was applied, the displacement response at failure reached −13.85 mm while the displacement at the left arch, where the second axle load was applied, reached −4.78 mm. Due to severe downward movement at the left and middle arches, the right arch experienced extreme uplift where the maximum displacement response reached 18.81 mm. This shows that the failure mechanism of the cellar system involves more than one cellar span. Note that the displacements were taken at the extrados of each arch.

To compare with the joint displacement vector plot shown in Fig. 9b, the joint normal displacement vectors of the middle arch at failure are presented in Fig. 11b. It is evident that the separation has extended both ways towards the springing level and towards the crown of the middle arch. Furthermore, the joint normal displacement at regions close to the right pier has reached a maximum value of 3.5 mm. The crack opening at the intrados of the arch close to the crown was also relatively large at 2.5 mm. Although no further inspection was conducted to measure the separation at the inside of the cellar, cracks perpendicular to the traffic direction at the middle wharf cellar was observed according to the Appendix A of the investigation report. Note that separations at the arch skewbacks were also found albeit small.

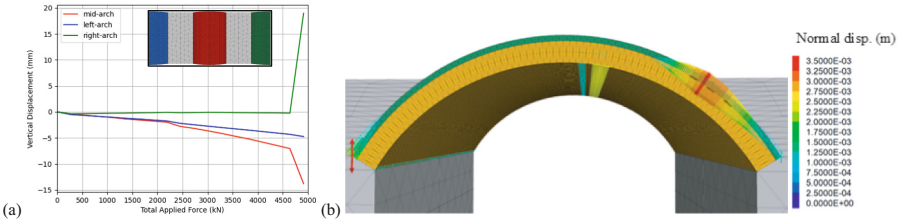

Fig. 11. (a) vertical displacement vs force increment and (b) normal displacement vector of the middle arch at failure

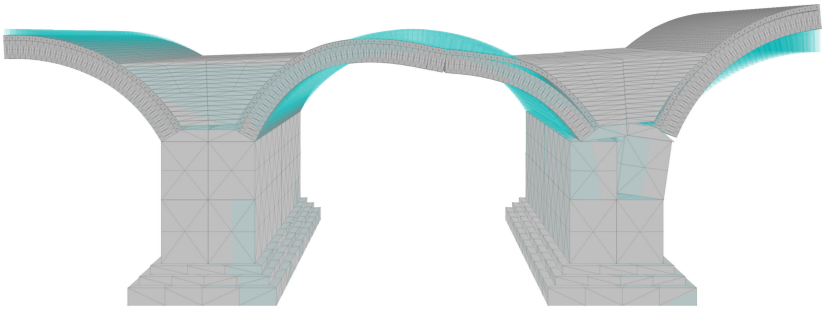

Fig. 12. Deformed shape of the wharf cellar model at failure load (magnified 10x)

The deformed shape of the wharf cellar is shown in Fig. 12 (magnified by a factor of 10) while the original shape is presented in a transparent shade of blue. Similar to what has been pointed out from the previous figures, a crack opening at the intrados closer to the crown of the middle arch was observed, while cracking at both the right and left side piers was also clearly shown. Rotation of the right side piers and separations at the right side arch skewbacks were found which was caused by the extreme uplift of the right side arch. In conclusion, the failure load and mechanism of the cellar system is simulated well where the spread of damage and displacement response at the onset of failure is clearly shown.

Note that similar to the numerical model in the investigation report, the loosely packed sand was assumed to be pre-loaded, hence no soft soil mechanism occurred at the cellar system which would have caused differential settlements at the piers of the cellar system which could cause a significantly different failure mechanism. It is also important to set a disclaimer that there are many simplifications considered in the numerical model such as the same crown height on each arches, the Boussinesq load dispersion, the blocky piers, and many more. Further calibrations of the numerical model with experimental tests are still needed and will be considered as the future work of this paper.

5 Conclusions

In this study, a micro-modelling approach for the safety assessment of an existing masonry wharf cellar system located in the *Kromme Nieuwegracht* canal in the city of Utrecht is introduced. A fast and robust geometry generation framework is created using *Rhino* + *Grasshopper*. The blocks are then imported to *3DEC* for the numerical analysis. Rigid block formulation is used where all deformations and system nonlinearities are lumped at the contacts between blocks. Backfill soil load is applied as a distributed dead load while the traffic load is applied as a dispersed load to the cellar's arch units according to the Boussinesq theory. The traffic load model in accordance with special emergency vehicle specified in the Dutch guideline is assessed for the wharf cellar structure. The heaviest axle of the traffic load model is applied at the crown of the middle arch while the second axle load is applied 4.2 m to the left side of the heaviest axle load.

The analysis results show that under the considered traffic load of the Dutch guideline for traffic loads in bridges, the deformation of the cellar system is overall still within the specified limit despite damage occurring at the intrados of the vault and the arch units close to the pier. The displacement response is also still relatively linear. The next task was to find the failure load and the governing failure mechanism by incrementally increasing the applied load beyond the full application. Failure was predicted for an ultimate load significantly larger than the normative load. At failure, the separation between the arch units was extended to the arch skewbacks on both sides of the middle arch while the failure mechanism at the crown of the left and right arches were different. The crown on the left side arch experienced sliding failure while the right side arch experienced a combination of sliding and separation at the bed joints of the horizontal units.

It is important to note that while this three-dimensional safety assessment framework can essentially be substituted by a two-dimensional model due to the 2-D load dispersion model, the intention to introduce the three-dimensional framework in this paper is to set a starting point of introducing a more sophisticated model where the load dispersion model is three-dimensional and that the cellar piers are discretized brick-by-brick as part of the future works. Moreover, the application of different traffic load positions and load scenarios according to the Dutch guidelines, and the variation of thickness of each arch in the vault structures will also be considered in order to simulate the actual condition of the wharf cellar system.

References

1. Brencich, A., Morbiducci, R.: Masonry arches: historical rules and modern mechanics. Int. J. Archit. Heritage **1**(2), 165–189 (2007)
2. Utrecht, G.: Kelders in het stadshart Utrecht. Gemeente Utrecht, Utrecht (2020). (in Dutch)
3. Korff, M., Hemel, M., Peters, D.: Collapse of the grimburgwal, a historic quay in Amsterdam. Proc. Inst. Civil Eng. Forensic Eng. **175**(4), 96–105 (2022)
4. NEN 8701+A1: Beoordeling van de constructieve veiligheid van een bestaand bouwwerk bij verbouwen en afkeuren – Belastingen. Nieuwe Europese Normen (2011). (in Dutch)
5. Sarhosis, V., De Santis, S., De Felice, G.: A review of experimental investigations and assessment methods for masonry arch bridges. Struct. Infrastruct. Eng. **12**(11), 1439–1464 (2016)

6. Tóth, A.R., Orbán, Z., Bagi, K.: Discrete element analysis of a stone masonry arch. Mech. Res. Commun. **36**, 469–480 (2009)
7. Gobbin, F., De Felice, G., Lemos, J.V.: A discrete element model for masonry vaults strengthened with externally bonded reinforcement. Int. J. Archit. Heritage **15**(12), 1959–1972 (2021)
8. Lemos, J.V., Gobbin, F., Forgács, T., Sarhosis, V.: Discrete element modelling of masonry arch bridges, arches, and vaults. In: Milani, G., Sarhosis, V. (eds) From Corbel Arches to Double Curvature Vaults. Springer, Cham (2022)
9. NEN-EN 1991-2:2021, Eurocode 1 - Actions on structures - Part 2: Traffic loads on bridges and other civil engineering works, European Committee for Standardization:Brussels (2021)
10. Royal Haskoning, D.H.V.: Verificatieberekening kelder Kromme Nieuwegracht te Utrecht. RHDHV, Utrecht (2021). (in Dutch)
11. NPR 9998:2020: Assessment of structural safety of buildings in case of erection, reconstruction and disapproval - Induced earthquakes - Basis of deisgn, actions, and resistances. Stichting Koninklijk Nederlands Normalisatie Instituut (2020)
12. Cundall, P.: A computer model for simulating progressive large-scale movements in blocky rock systems. In: Proceedings of the International Symposium on Rock Fractures. ISRM, France (1971)
13. Itasca Consulting Group, Inc, Three-Dimensional Distinct Element Code, Ver. 7.0, Minneapolis: Itasca (2020)
14. Lemos, J.V.: Discrete element modeling of the seismic behavior of masonry construction. Buildings **9**(2), 43–54 (2019)
15. Centre for Civil Engineering Research and Codes, C: Structural Masonry: An Experimental/ Numerical Basis for Practical Design Rules. CRC Press:Netherlands (2014)
16. Choo, B., Coutie, M., Gong, N.: Finite-element analysis of masonry arch bridges using tapered elements. Proc. Inst. Civil Eng. **91**(4), 755–770 (1991)
17. Ni, P., Mangalathu, S., Song, L., Mei, G., Zhao, Y.: Displacement-dependent lateral earth pressure models. J. Eng. Mech. **144**(6), 1–12 (2018)